Experimental Shot-by-Shot Estimation of Quantum Measurement Confidence

Ivan A. Burenkov[1,2,*] N. Fajar R. Annafianto,[2] M. V. Jabir,[2] Michael Wayne,[1,2]
Abdella Battou,[2] and Sergey V. Polyakov[2,3]

[1]*Joint Quantum Institute and University of Maryland, College Park, Maryland 20742, USA*
[2]*National Institute of Standards and Technology, Gaithersburg, Maryland 20899, USA*
[3]*Physics Department, University of Maryland, College Park, Maryland 20742, USA*

We demonstrate the single-shot confidence estimation for individual quantum measurement outcomes using the continuous measurement theory of the quantum counting process applied to the quantum state identification problem. We experimentally obtain single-shot and average confidences for quantum measurements and show that they favorably compare to that of the idealized classical measurement. Finally, we demonstrate that single-shot confidence estimations correctly represent observed experimental outcomes for a large ensemble of measurements.

Measurements connect quantum mechanics to the "classical" world. Yet, unless the measured quantum state belongs to a known orthogonal set, it is not possible to measure the state of a quantum system with a single-shot measurement. Thus, without some prior knowledge, the state cannot be determined with full certainty. Because of the inherent uncertainty of all measurements, only partial information about the observed quantum system is typically available [1–3]. Understanding and practically attaining the fundamental limits on the achievable accuracy is the paramount problem in quantum measurement. It has been shown that quantum measurements can significantly surpass classical measurements and, in some cases, asymptotically approach the fundamental limits of accuracy, see, for example, [4–10]. Generally, because quantum measurements are probabilistic, these efforts describe probabilities for experimental outcomes, not exactly what will occur in each measurement. Here, for the first time, we experimentally obtain confidence estimates for each individual measurement outcome and verify that each single-shot estimate correctly predicts the accuracy of the corresponding act of measurement.

Identifying randomly distributed quantum states from a known set of states is an important application of quantum measurements [4,11–13]. Because perfect identification of nonorthogonal states is impossible, a certain figure of merit is identified, and the measurement is optimized accordingly [11,14–16]. One such figure of merit is the probability to obtain the correct result without learning which identification is correct and which is wrong. A quantum measurement can be optimized so that this probability can surpass the so-called shot-noise limit of the ideal classical measurements, [5,6,9,17–28]. Other figures of merit exist. For instance, knowing which states in particular were identified without error may be desired. Theoretically,

error-free identification is probabilistically possible, i.e., a measurement protocol which occasionally fails, but when the protocol is successful, the result is always correct [29–31]. The figure of merit, then, is the probability of a successful, conclusive result. In practice, this so-called unambiguous state discrimination is not completely error free due to experimental imperfections [32–36].

A shot-by-shot confidence estimation in quantum state discrimination measurements is a useful generalization [37]. Both the unambiguous discrimination of linearly independent states [31] (more generally, of states whose support does not overlap [38]) and the minimum-error discrimination when the average confidence is maximized [16] reduce to the maximum confidence problem. In general, the maximum confidence measurement strategy is not known for discriminating more than two states [39–41].

In this Letter, we experimentally obtain confidence estimations for individual, single-shot quantum measurements. We demonstrate higher single-shot and averaged fidelity between the measured and the input states than that of the idealized classical measurement. We verify that single-shot confidence estimations experimentally match the observed success probabilities averaged over a large ensemble of measurements. The knowledge of the confidence of each act of measurement independently generalizes state identification problems and opens multiple possibilities in applied quantum measurement; for instance, it could enhance the measurement accuracy beyond classical means. It can also be used for advanced error correction and the self-diagnostics of a quantum measurement system.

Consider a single-shot state identification problem where only a single copy of the input state ϕ_s, $s \in 1, ..., M$ is available. Without the loss of generality, we assume that $\{\phi_s\}$ are in a single spatial mode and focus on temporal

dynamics. We take an explicit advantage of the fact that the continuous measurement of the state $|\phi\rangle$ is made over time T, where T is the duration of the input pulse. In the continuous limit, the measurement operator is (cf. [42–44])

$$\hat{\pi} = \lim_{dt \to 0} (\hat{C}_T \hat{U}_T \times \ldots \times \hat{C}_{2dt} \hat{U}_{2dt} \hat{C}_{dt} \hat{U}_{dt}), \quad (1)$$

where $\hat{U}$ denotes a transformation of the state, such as coherent displacement, and $\hat{C}$ describes photon counting on the interval dt. The choice of unitary transformations applied to a measured state $\{\hat{U}\}$ depends on the choice of the figure of merit of the measurement and the set of ϕ_s. Owing to the probabilistic nature of photon detection, the outcome of this continuous measurement is unique for each individual measurement attempt. It consists of the history of all measurements λ and all applied transformations: $\mathbb{Z}[0, t] = (\lambda_t, \ldots, \lambda_{2dt}, \lambda_{dt}; \hat{U}_t, \ldots, \hat{U}_{2dt}, \hat{U}_{dt})$, where $t < T$ [45]. When $t = T$, the measurement history is complete, otherwise, the record is incomplete. The conditional probability $p(\mathbb{Z}[0, t]|\phi_s)$ that a given measurement record $\mathbb{Z}[0, t]$ occurs if the input was in a state ϕ_s, can be computed using a model of the experiment. The model can account for experimental imperfections, such as non-ideal displacement and dark noise of the detector. The probability $p(\phi_s|\mathbb{Z}[0, t])$ that the input state is ϕ_s once the record $\mathbb{Z}[0, t]$ can be obtained using the Bayes formula

$$p(\phi_s|\mathbb{Z}[0, t]) = \frac{p(\mathbb{Z}[0, t]|\phi_s)\tilde{p}_s}{p(\mathbb{Z}[0, t])}, \quad (2)$$

where $\vec{P}_0 = \{\tilde{p}_s\}$ is the probability to encounter an input state ϕ_s, which is typically known from the formulation of the problem. We form a vector of confidences, using probability values $\vec{P} = \{p(\phi_s|\mathbb{Z}[0, t])\}$, whose components represent our best knowledge about the input state during $(t < T)$ and after $(t = T)$ the measurement. We experimentally measure $\mathbb{Z}[0, T]$ and obtain $\vec{P}$. See Supplemental Material [46] for examples of measurement strategies, $\mathbb{Z}[0, T]$, models that relate $\mathbb{Z}[0, T]$ to $\vec{P}$, and corresponding $\vec{P}$.

In our experimental example, we find shot-to-shot confidences in an optical continuous quantum measurement, maximizing the probability of the successful detection. The input is in one of $M = 4$ flat-top equiprobable coherent states that differ by phase: $|\phi_s\rangle = |\alpha e^{is2\pi/M}\rangle$, Fig. 1(a). The measurement consists of the coherent displacement stage and the single-photon detector, Fig. 1(c). Because we are interested in maximizing the probability of correct identification, the displacement adapts according to the following rules. At $t = 0$, we set the local oscillator (LO) to state h_0 that corresponds to displacing the state with the highest initial probability $\max(\tilde{p}_s)$ to vacuum. Here, the initial vector is set to equal probabilities $\vec{P}(0) = \{0.25, 0.25, 0.25, 0.25\}$, which is a
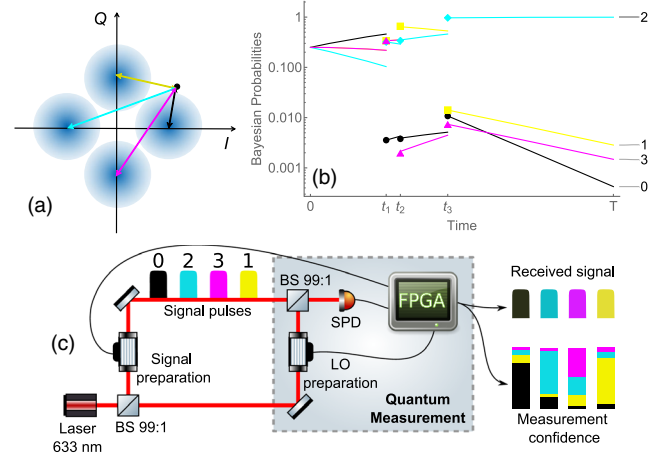
FIG. 1. (a) A constellation diagram of $M = 4$ coherent states that differ by phase. Fuzzy circles represent uncertainty due to shot noise. Black dot—a possible outcome of a homodyne measurement. Arrows—difference between the value obtained with a homodyne and the expected states (used in calculating $\vec{P}_C$, see text); (b) an example of the experimentally measured $\vec{P}(t)$ in a single-shot measurement. Here, single photon detections occur three times at t_1, t_2, and t_3; (c) Experimental setup. For each signal pulse, the quantum measurement determines the most likely input state and the confidence of discrimination (Bayesian probability of each of the possible states based on the measurement record, see text). The optical input for system efficiency characterization is defined at the input port of the fiber beam splitter (BS) used for displacement and includes detection efficiency of the single-photon detector (SPD).

common situation for data communication applications. Because our states are equiprobable, we chose $h_0 = 0$. During the measurement, we use the incomplete detection record $\mathbb{Z}[0, t]$ to update the hypothesis. The adaptive algorithm is discussed in detail in the Supplemental Material [46]. Unless a photon is detected, components of the vector $\vec{P}$ evolve continuously. Once a photon is detected at t_j, the probability $p_{h_{j-1}}$ gets reduced, while other probabilities become higher [51], Fig. 1(b). Evidently, with ideal displacement and noiseless detection the conditional probability that the input state is h_{j-1} reduces to zero if a photon is detected at t_j, however, ideal displacement cannot be achieved in a practical measurement. According to the adaptive algorithm, updates of h only occur when a photon is detected at time t_j [22,27,51]. Note that the chance to detect more than one photon during $dt \to 0$ is negligible for weak coherent states, i.e., $\lambda = \{0, 1\}$. Thus, in our case, the measurement record gives the exact times of photodetection events and applied unitary transformations (displacements). The updates of h and corresponding unitary transformations $\hat{U}$ follow the Bayesian inference, with the incomplete record $\mathbb{Z}[0, t_j]$. At the end of the measurement $t = T$, we obtain $\mathbb{Z}[0, T] = (t_1, t_2, \ldots, t_f; \hat{U}_{h_0}, \hat{U}_{h_1}, \ldots, \hat{U}_{h_f})$ and the vector $\vec{P}$. Prior to this Letter, the

FIG. 2. A visual comparison of single-shot confidence estimates in quantum and classical measurements. Left: the original image of 128×128 pixels where four primary (black, yellow, cyan, and magenta) colors correspond to the different symbols $|\phi_s\rangle$. Middle: the same image experimentally obtained from continuous quantum measurement record. Right: the same image reconstructed from the simulated ideal homodyne measurement. The color for each pixel is calculated as a sum of primary colors weighted with the probabilities $\vec{P}$ (middle) and $\vec{P}_C$ (right) of corresponding symbols.

measurement records $\mathbb{Z}$ and numerical values of $\vec{P}$ components were inaccessible. Yet, because the exact pattern of photon detections is unique to each measurement "shot," due to the stochastic nature of photon detection, the record $\mathbb{Z}$ and the values of $\vec{P}$ are also unique to each shot. As we experimentally show, these numerical values represent our best knowledge of the input state and describe the individual reliability for each act of measurement. Examples of raw experimental data and corresponding temporal evolution of $\vec{P}(t)$ are available in the Supplemental Material [46].

$\vec{P}$ can be generalized to classical measurements. The ideal homodyne measurement is limited by shot noise. Therefore, a measurement of the state of the input field [I and Q, Fig. 1(a)] does not determine the input state with full certainty [52]. A vector $\vec{P}_C$ for each classical measurement outcome $\{I, Q\}$ can be determined as [cf. Eq. (2)]

$$p_C(\phi_s|I, Q) = \frac{p(I, Q|\phi_s)\tilde{p}_s}{\sum_{j=1}^{M} p(I, Q|\phi_j)\tilde{p}_j}, \qquad (3)$$

where $p(I, Q|\phi_s) = \exp[-(I - \alpha\cos\theta_s)^2 - (Q - \alpha\sin\theta_s)^2]$. Therefore, the uncertainty of the classical measurement of I and Q results in the uncertainty of state discrimination, where $\vec{P}_C$ represents our knowledge about the input state in a full analogy with the quantum measurement.

Figure 1(c) shows our experiment. A laser at 632 nm is used to prepare both input and the LO states. Phases are adjusted with acousto-optic modulators [53]. The field programmable gate array (FPGA) generates rf pulses at 80 MHz to set the appropriate phase for both signal and LO, runs the maximal likelihood estimation algorithm, and reports values of $\vec{P}$ for each measurement. The displacement occurs on a $\mathcal{T}:\mathcal{R} \approx 99:1$ beamsplitter. The single-photon detector is a commercial silicon avalanche photodiode. The mean photon number of the input state is measured to be

2.68 photons/pulse (2 photons/pulse after adjustment for system efficiency), and the LO is ≈ 100 times stronger than the input state before the beamsplitter. The setup is interferometrically stabilized with a 795 nm auxiliary laser locked to a rubidium atomic line. The measurement and locking cycles are interspersed with a duty factor of 50%. The symbol duration is $T = 65.4\ \mu$s. The measured visibility of the interferometer is 99.7%. The system efficiency is 74.5(6)%, which includes propagation loss of 11.4(5)% and detection efficiency of 84.0(3)%.

In our experiment, we send user-defined $128 \times 128 = 16\,384$ pixel images and identify 16 384 states using quantum measurement. Each pixel represents one input state s, and each of the four primary colors (black, yellow, cyan, and magenta) corresponds to an input symbol $|\phi_0\rangle, \ldots, |\phi_3\rangle$ of the alphabet, color $= \delta_{0,s} \times$ black $+ \delta_{1,s} \times$ yellow $+ \delta_{2,s} \times$ cyan $+ \delta_{3,s} \times$ magenta, where δ is the Kronecker delta. Every possible input symbol is sent 4096 times, Fig. 2 (left). Upon single-shot measurements, the same image is reconstructed using the confidence vector $\vec{P}$, such that color $= p_0 \times$ black $+ p_1 \times$ yellow $+ p_2 \times$ cyan $+ p_3 \times$ magenta, see Fig. 2 (middle). Received pixels can have an arbitrary color, because all four components of $\vec{P}$ may be nonzero. If a measurement determines the input state correctly and with low uncertainty, pixels on the reconstructed image are almost indistinguishable from the original. Some pixels appear as off color "polka dots" in Fig. 2 (middle). Lower-confidence, but correct outcomes resemble the expected primary color, but appear off color. Lower-confidence, incorrect outcomes are also off color, and they do not resemble the expected primary color. Finally, high-confidence incorrect outcomes are close to the unexpected primary color. In our case, most of the pixels are close to the primary color, because the overall error rate in this experiment is fairly low: $\approx 4.7\%$. To compare the accuracy of this measurement to an ideal classical
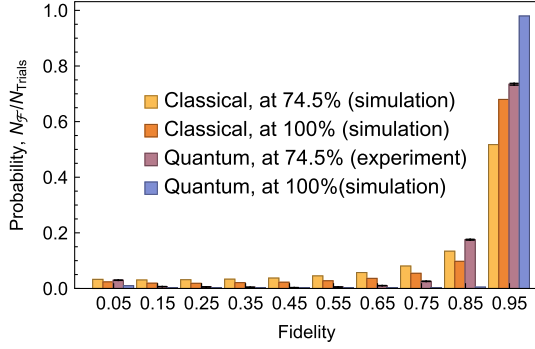
FIG. 3. Probability of the measurement outcome with a certain fidelity for faint input ($\langle n \rangle = 2.68$ photons per signal pulse) prepared in one of $M = 4$ states. Orange bars—simulation of the ideal homodyne receiver adjusted for system efficiency of 74.5%. Red bars—simulation of the ideal homodyne receiver. Purple bars—experimental data. Blue bars—simulation of the idealized experimental receiver. Histogram bin width is 0.1, bin center positions are shown on the horizontal axis.

measurement, we plot a simulated reconstructed image using the same input conditions and assuming the ideal shot-noise limited homodyne detector, Fig. 2 (right). We see a higher number of lower-confidence measurements. This result is not surprising, because our measurement method is not constrained by the shot noise, while classical measurement is.

The single-shot fidelity estimate can be introduced as $\mathcal{F} = \vec{P}\,\vec{S}$, where $\vec{S}$ is the input state (when $|\psi_s\rangle$ is sent, the components of $\vec{S}$ are $S_j = \delta_{j,s}$). For a large ensemble of measurements, we group all estimates $\mathcal{F}$ into 10%-wide bins. We compute and plot $N_{\mathcal{F}}$, the total number of trials whose fidelity estimate falls into each bin normalized on total number of trials N_{Trials}, Fig. 3. We compare the experimental data with the simulated ideal homodyne measurement with unit efficiency, simulated ideal homodyne with the same system efficiency as our experiment, and the simulated ideal displacement-based adaptive quantum measurement with unit efficiency using the same input conditions. In Fig. 3, we see that our measurement produces high fidelity ($\mathcal{F} > 0.9$) results about 1.06 times more often than the ideal classical measurement with unity efficiency and 1.36 times more often than the ideal classical measurement with matching system efficiency. Note that the number of measurement outcomes with lower fidelity is significantly lower for our measurement in comparison to the ideal homodyne measurement. In particular, the homodyne measurement returns almost an order of magnitude more outcomes with $\mathcal{F} \approx 0.5$. Therefore, the quantum measurement unconditionally provides more definitive information about the input state. In aggregate, the average fidelity of our quantum measurement is $\langle \mathcal{F} \rangle = 0.874(1)$, whereas the average fidelities of the idealized classical measurements are $\langle \mathcal{F}_C \rangle = 0.854(1)$ and $0.782(1)$ for unit and matching experimental system efficiencies,
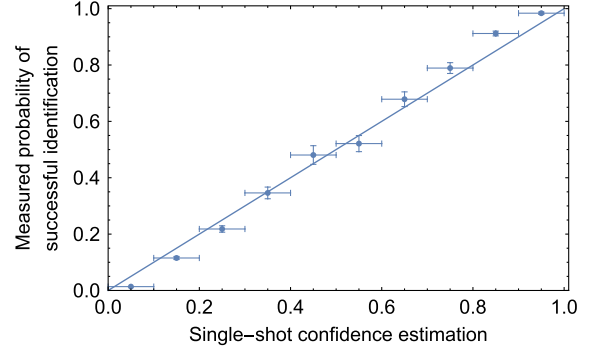
FIG. 4. Experimentally measured single-shot confidence vs the experimental ensemble average probability of a successful state discrimination obtained for faint input ($\langle n \rangle = 2.68$ photons per signal pulse) prepared in one of $M = 4$ states. Vertical error bars correspond to 1 standard deviation, horizontal error bars show histogram bin size.

respectively. The ideal displacement-based measurement would give $\langle \mathcal{F} \rangle = 0.981(1)$, while the fidelity of the ideal quantum measurement can be bounded from above by 0.998 under our experimental conditions, see Supplemental Material [46].

In practice, $\vec{S}$ is *a priori* unknown. Now, we experimentally show that $\vec{P}$ represents our best knowledge about the input state. For a large ensemble of measurements, we see how often the true state of the input matches a measured state component whose single-shot probability falls into a certain range. For all the components p of the $\vec{P} = \{p_0, \ldots, p_3\}$, we define the 10%-wide bins, and we compute the number of successful and unsuccessful state identifications. The probability of a successful identification q is $q(p) = N_{\text{correct}}/(N_{\text{correct}} + N_{\text{incorrect}})$, where $N_{\text{correct,incorrect}}$ are the number of correct (incorrect) detections. We plot q as a function of p, (Fig. 4). Experimentally, we see that the ensemble average discrimination error probabilities observed for an ensemble of single-shot measurements q are equal to the observed single-shot confidence estimations p, Fig. 4. Remarkably, this equality is true for any value of p, including the measurements with very high confidence estimation $p \approx 1$ and low confidence estimation $p \approx 0$. An obvious use of p is to set a confidence threshold $p_{\text{th}} < 1$ and reject the measurements where $\max(p_j) < p_{\text{th}}$. This use of p is similar to the unambiguous state discrimination, but the confidence threshold is below unity. The experimentally measured error rate for nominally unambiguous measurements in [35] and [36] are $\approx 2.5\%$ and $\approx 1\%$, respectively, similar to the verified single-shot confidence of our experiment. A very important, less obvious result is that the smaller components of $\vec{P}$, i.e., the components which would not be picked in a maximal likelihood analysis, successfully determine the input state with the same probability as that obtained from single-shot measurement. Thus, we verified that

$\vec{P}$ represents the best knowledge about the input state, for each single-shot measurement record. A deviation from the straight line can be used to identify either a wrong measurement model and/or incorrectly assigned $\vec{P}(0)$.

In conclusion, this Letter is the first experimental measurement of the single-shot confidence estimates. Here, confidences are obtained for an example of quantum state identification by taking advantage of continuous quantum measurement. We have shown that the fidelity of the received states is significantly higher in our experiment when compared to the ideal classical measurement. We have also shown that the Bayesian probability estimates of successful detection correctly identify success probabilities found by ensemble averaging. Fundamentally, this experiment illustrates some of the principles of quantum Bayesianism [54], whereby the information obtained in a quantum measurement depends on the agent that performs the measurement (in our example, either a classical or a quantum measurement device) and on its measurement outcomes (in our example, the measurement record). We have shown that the continuous measurement offers a significant advantage by making the single-shot confidence estimation available and have demonstrated that both prior knowledge about measured quantum sates and the physical model of the measurements used to identify these states are close to the actual conditions. In practice, the single-shot confidence estimation vector can be used to discard low confidence quantum measurements, correct measurement errors, as well as detect eavesdropping and distortion specifically in communication channels.

---

[*]ivan.burenkov@gmail.com

[1] A. Peres and W. K. Wootters, Phys. Rev. Lett. **66**, 1119 (1991).

[2] C. A. Fuchs, arXiv:quant-ph/9601020.

[3] J. M. Geremia, Phys. Rev. A **70**, 062303 (2004).

[4] A. Kholevo, *Probabilistic and Statistical Aspects of Quantum Theory*, North-Holland Series in Statistics and Probability (North-Holland Publishing Company, Amsterdam, 1982).

[5] R. S. Kennedy, Research Laboratory of Electronics, MIT, Technical Report No. 108, 1972, https://dspace.mit.edu/handle/1721.1/56346.

[6] S. J. Dolinar, Research Laboratory of Electronics, MIT, Technical Report No. 111, 1973, https://dspace.mit.edu/handle/1721.1/56414.

[7] S. L. Braunstein and C. M. Caves, Phys. Rev. Lett. **72**, 3439 (1994).

[8] M. P. da Silva, S. Guha, and Z. Dutton, Phys. Rev. A **87**, 052320 (2013).

[9] F. Becerra, J. Fan, G. Baumgartner, J. Goldhar, J. Kosloski, and A. Migdall, Nat. Photonics **7**, 147 (2013).

[10] M. T. DiMario and F. E. Becerra, Phys. Rev. Lett. **125**, 120505 (2020).

[11] C. W. Helstrom, J. Stat. Phys. **1**, 231 (1969).

[12] A. Holevo, *Statistical Structure of Quantum Theory*, Lecture Notes in Physics Monographs (Springer, Berlin, Heidelberg, 2003).

[13] S. Barnett, *Quantum Information*, Oxford Master Series in Physics (Oxford University Press, Oxford, New York, 2009).

[14] E. B. Davies and J. T. Lewis, Commun. Math. Phys. **17**, 239 (1970).

[15] K. Kraus, A. Böhm, J. D. Dollard, and W. H. Wootters, *States, Effects, and Operations Fundamental Notions of Quantum Theory* (Springer, Berlin, Heidelberg, 1983), Vol. 190, https://doi.org/10.1007/3-540-12732-1.

[16] S. M. Barnett and S. Croke, Adv. Opt. Photonics **1**, 238 (2009).

[17] R. S. Bondurant, Opt. Lett. **18**, 1896 (1993).

[18] S. Izumi, M. Takeoka, K. Wakui, M. Fujiwara, K. Ema, and M. Sasaki, Sci. Rep. **8**, 2999 (2018).

[19] R. Blume-Kohout, S. Croke, and M. Zwolak, arXiv:1201.6625.

[20] F. Becerra, J. Fan, and A. Migdall, Nat. Photonics **9**, 48 (2015).

[21] J. Chen, J. L. Habif, Z. Dutton, R. Lazarus, and S. Guha, Nat. Photonics **6**, 374 (2012).

[22] I. A. Burenkov, O. V. Tikhonova, and S. V. Polyakov, Optica **5**, 227 (2018).

[23] M. T. DiMario and F. E. Becerra, Phys. Rev. Lett. **121**, 023603 (2018).

[24] M. DiMario, L. Kunz, K. Banaszek, and F. Becerra, npj Quantum Inf. **5**, 65 (2019).

[25] M. L. Shcherbatenko, M. S. Elezov, G. N. Goltsman, and D. V. Sych, Phys. Rev. A **101**, 032306 (2020).

[26] S. Izumi, J. S. Neergaard-Nielsen, and U. L. Andersen, Phys. Rev. Lett. **124**, 070502 (2020).

[27] I. A. Burenkov, M. V. Jabir, A. Battou, and S. V. Polyakov, PRX Quantum **1**, 010308 (2020).

[28] M. V. Jabir, I. A. Burenkov, N. F. R. Annafianto, A. Battou, and S. V. Polyakov, OSA Continuum **3**, 3324 (2020).

[29] G. Jaeger and A. Shimony, Phys. Lett. A **197**, 83 (1995).

[30] A. Peres and D. R. Terno, J. Phys. A **31**, 7105 (1998).

[31] A. Chefles, Phys. Lett. A **239**, 339 (1998).

[32] B. Huttner, A. Muller, J. D. Gautier, H. Zbinden, and N. Gisin, Phys. Rev. A **54**, 3783 (1996).

[33] R. B. M. Clarke, A. Chefles, S. M. Barnett, and E. Riis, Phys. Rev. A **63**, 040305(R) (2001).

[34] J. Mizuno, M. Fujiwara, M. Akiba, T. Kawanishi, S. M. Barnett, and M. Sasaki, Phys. Rev. A **65**, 012315 (2001).

[35] F. E. Becerra, J. Fan, and A. Migdall, Nat. Commun. **4**, 2028 (2013).

[36] S. Izumi, J. S. Neergaard-Nielsen, and U. L. Andersen, PRX Quantum **2**, 020305 (2021).

[37] S. Croke, E. Andersson, S. M. Barnett, C. R. Gilson, and J. Jeffers, Phys. Rev. Lett. **96**, 070401 (2006).

[38] T. Rudolph, R. W. Spekkens, and P. S. Turner, Phys. Rev. A **68**, 010301(R) (2003).

[39] P. J. Mosley, S. Croke, I. A. Walmsley, and S. M. Barnett, Phys. Rev. Lett. **97**, 193601 (2006).

[40] S. Croke, P. J. Mosley, S. M. Barnett, and I. A. Walmsley, Eur. Phys. J. D **41**, 589 (2007).

[41] G. A. Steudle, S. Knauer, U. Herzog, E. Stock, V. A. Haisler, D. Bimberg, and O. Benson, Phys. Rev. A **83**, 050304(R) (2011).

[42] C. Gardiner, *Quantum Noise* (Springer Verlag, Berlin, 1991).

[43] H. M. Wiseman and G. J. Milburn, Phys. Rev. A **47**, 642 (1993).

[44] A. C. Doherty, S. M. Tan, A. S. Parkins, and D. F. Walls, Phys. Rev. A **60**, 2380 (1999).

[45] M. Srinivas and E. Davies, Opt. Acta **28**, 981 (1981).

[46] See Supplemental Material at http://link.aps.org/supplemental/10.1103/PhysRevLett.128.040404 for examples of measurement strategies, $\mathbb{Z}[0,T]$, models that relate $\mathbb{Z}[0,T]$ to $\vec{P}$, and corresponding $\vec{P}$, the adaptive algorithm, and examples of raw experimental data and corresponding temporal evolution of $\vec{P}(t)$ and derivation of fidelity bound, which includes Refs. [47–50].

[47] I. Ivanovic, Phys. Lett. A **123**, 257 (1987).

[48] D. Dieks, Phys. Lett. A **126**, 303 (1988).

[49] A. Peres, Phys. Lett. A **128**, 19 (1988).

[50] C. W. Helstrom, J. Stat. Phys. **1**, 231 (1969).

[51] C. R. Müller and C. Marquardt, New J. Phys. **17**, 032003 (2015).

[52] J. P. Gordon, Proc. IRE **50**, 1898 (1962).

[53] E. A. Donley, T. P. Heavner, F. Levi, M. O. Tataw, and S. R. Jefferts, Rev. Sci. Instrum. **76**, 063112 (2005).

[54] C. A. Fuchs, arXiv:1003.5209.